Rodríguez-Millán, M., García-González, D., Arias, A. (2020) Failure Behavior of Aluminum Alloys Under Different Stress States. In: Voyiadjis, G.Z. (eds.) *Handbook of Damage Mechanics.* New York*:* Springer, 1-25.

DOI: https://doi.org/10.1007/978-1-4614-8968-9_68-1

Failure Behavior of Aluminum Alloys Under Different Stress States

M. Rodríguez-Millán, D. Garcia-Gonzalez, and A. Arias

Contents

Abstract

This chapter analyzes the current state of the art on ductile damage in aluminum alloys. To this end, the main experimental methodologies developed to date for this purpose are identified and introduced. The analysis of failure in this type of materials is rather complex and requires the consideration of two parameters dependent on the stress state: triaxiality and Lode parameter. Different values of triaxiality and Lode parameter can be obtained by properly defining the testing load and the specimen geometry. These results are especially interesting to feed constitutive and failure models such as the Johnson-Cook model or the Bai-Wierzbicki model. This chapter focuses on different stress states associated to different Lode parameter and triaxialities: tension, compression, shear, and combined tension-torsion. To this end, a wide variety of testing specimens are introduced describing their relation to these parameters. Thus, this content aims at providing guidance for characterization testing of ductile fracture of metals and further calibration of failure models.

M. Rodríguez-Millán (✉)
Department of Mechanical Engineering, University Carlos III of Madrid, Madrid, Spain
e-mail: mrmillan@ing.uc3m.es

D. Garcia-Gonzalez · A. Arias
Department of Continuum Mechanics and Structural Analysis, University Carlos III of Madrid, Madrid, Spain
e-mail: danigarc@ing.uc3m.es; aariash@ing.uc3m.es

The chapter first introduces fundamental concepts, then a brief description of failure models, and, finally, a detailed methodological description on the characterization of metals at different triaxialities and Lode parameters.

Keywords

Triaxiality · Lode parameter · Johnson and Cook · Ductile failure criterion · Tension stress · Bridgman · Grooved flat specimen · Dog-bone specimen · Uniaxial compression · Shear specimens · Arcan specimens · Equi-biaxial test · Butterfly specimen · Punch test · Hasek tests · Modified shear specimen · Double notched tube specimen · 5754-H111 · 6082-T6;2024-T3 · Modified Lindholm specimen

Introduction

In the last 60 years, ductile failure in metallic materials has been studied due to its importance in the design of mechanical and structural components. When plastic strain reaches a certain limit value, there is a loss of the capacity to support loads giving rise to the phenomenon of ductile failure. In this regard, large plastic deformations around crystalline defects lead to instabilities resulting into the failure phenomenon. The ductile fracture in metals is based on voids distributed within the material and nucleated during deformation that grow together (*coalescence*) to form a continuous path to fracture (Garrison Jr and Moody 1987). The stages at which the fracture phenomenon occurs can be divided into:

- *Vacuum Initiation*. It occurs by separation of the particle-matrix interface and by fracture of the particle. The deformation to which the nucleation of voids occurs is very dependent on the stress state (Garrison Jr and Moody 1987).
- *Growth of Voids*. After nucleation, the voids expand with a certain volume and shape. The development of this process is governed by plastic deformation. Microvacuum growth models include McClintock's work (McClintock et al. 1966; McClintock 1968) in which the importance of high triaxialities in void growth is highlighted.
- *Vacuum Coalescence*. The voids are joined in such a way that material fracture occurs.

In this regard, the stages involved in failure deformation are highly dependent on the stress state according to various studies (Brigdman 1935; Hancock and MacKenzie 1975; Bao 2005; Barsoum and Faleskog 2007a; Rice and Tracery 1969). One mechanical variable to define the stress state is the hydrostatic pressure, defined by:

$$p = -\sigma_m = -\frac{1}{3}I_1 = -\frac{1}{3}\sigma_{ij} = -\frac{1}{3}(\sigma_1 + \sigma_2 + \sigma_3) \quad (1)$$

where σ_{ij} are the stress tensor components; σ_1, σ_2 and σ_3 are the principal stress components; and I_1 is the first invariant of the stress tensor. The hydrostatic stress is insufficient to characterize the stress state, so it is necessary to introduce the deviatoric stress components. Thus, denoting σ'_{ij} as the deviatoric stress and σ'_1, σ'_2 and σ'_3 as its principal components, then

$$\sigma'_{ij} = \sigma_{ij} - \sigma_m \, \delta_{ij} \tag{2}$$

where δ_{ij} is the unit matrix. The invariants of the deviatoric stress tensor can be expressed as:

$$\begin{gathered} J_1 = 0 \\ J_2 = \frac{1}{2}\sigma'_{ij}\sigma'_{ji} = -\left(\sigma'_1\sigma'_2 + \sigma'_2\sigma'_3 + \sigma'_3\sigma'_1\right) = \frac{1}{6}\left[(\sigma_1 - \sigma_2)^2 + (\sigma_2 - \sigma_3)^2 + (\sigma_3 - \sigma_1)^2\right] \\ J_3 = \det\left(\sigma'_{ij}\right) = \frac{1}{3}\sigma'_{ij}\sigma'_{jk}\sigma'_{ki} = \sigma'_1\sigma'_2\sigma'_3 \end{gathered} \tag{3}$$

and the effective or equivalent stress is defined as:

$$\overline{\sigma} = \sqrt{3\,J_2} \tag{4}$$

The state of principal stresses can be geometrically represented as a vector in a three-dimensional space, where principal stresses are taken as Cartesian coordinates (Fig. 1a). The vector $\overrightarrow{OP}$ is the principal stress vector which represents the stress state (σ_1, σ_2, σ_3). This vector can be broken down into two components: the vector $\overrightarrow{ON}$, which corresponds to the state of hydrostatic stress, and the vector $\overrightarrow{NP}$, which represents the deviatoric term (Eq. 5):

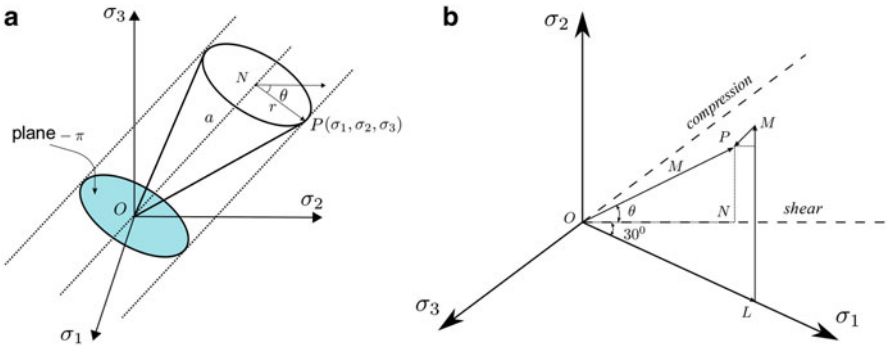

Fig. 1 (**a**) Stress states with the same triaxiality, (**b**) deviatoric stress tensor vector and its components along the projected axes

$$\begin{aligned}\overrightarrow{ON} &= a = \sqrt{3}\sigma_m \\ \overrightarrow{NP} &= r = \sqrt{\frac{2}{3}}\,\overline{\sigma}\end{aligned} \tag{5}$$

To distinguish different stress states having the same hydrostatic stress ratio, the location in the plane π of the projection point P is considered (Fig. 1b). Since each tension axis is inclined relative to the deviatoric plane at an angle of 120° at origin, each projection along the axes is $\sqrt{\frac{2}{3}}$ times the actual length. So, the vector lengths in the deviatoric plane are: $\overrightarrow{OL} = \sqrt{\frac{2}{3}}\,\sigma_1$, $\overrightarrow{LM} = \sqrt{\frac{2}{3}}\,\sigma_2$, and $\overrightarrow{MP} = \sqrt{\frac{2}{3}}\,\sigma_3$. Considering $\sigma_1 > \sigma_2 > \sigma_3$, the vector $\overrightarrow{OP}$ can be divided with respect to the horizontal and vertical components as:

$$\begin{aligned}\overrightarrow{ON} &= \overrightarrow{OL}\cdot\cos 30 - \overrightarrow{MP}\cdot\cos 30 = \sqrt{\frac{2}{3}}\sigma_1\cdot\sqrt{\frac{3}{2}} - \sqrt{\frac{2}{3}}\sigma_3\cdot\sqrt{\frac{3}{2}} = \frac{\sigma_1-\sigma_2}{\sqrt{2}} = r\cos\theta \\ \overrightarrow{PN} &= \overrightarrow{LM} - \overrightarrow{MP}\cdot\sin 30 - \overrightarrow{OL}\cdot\sin 30 = \sqrt{\frac{2}{3}}\sigma_2 - \sqrt{\frac{2}{3}}\sigma_1\cdot\frac{1}{2} - \sqrt{\frac{2}{3}}\sigma_3\cdot\frac{1}{2} \\ &= \frac{2\sigma_2-\sigma_1-\sigma_3}{\sqrt{2}} = r\sin\theta\end{aligned} \tag{6}$$

Consequently, **triaxiality** is defined as the ratio between hydrostatic stress and equivalent stress as reflected in Eq. 7.

$$\eta = \frac{\sigma_m}{\overline{\sigma}} = \frac{\frac{1}{3}I_3}{\sqrt{3J_2}} = \frac{\sqrt{2}}{3}\frac{a}{r} \tag{7}$$

Triaxiality has often been used in ductile fracture as a measure of material ductility and has been directly correlated with failure deformation by numerous researchers (McClintock et al. 1966; Rice and Tracery 1969; Johnson and Cook 1985; Bao and Wierzbicki 2004a).

Bao and Wierzbicki (Bao and Wierzbicki 2004a, b; Bao 2003), as well as Barsoum and Faleskog (2007a), concluded that triaxiality alone was not sufficient to properly describe the behavior of the material at failure. Therefore, they introduced a second parameter, stress state indicator, **Lode's parameter**, which is defined as:

$$\frac{2\sigma_2-\sigma_1-\sigma_3}{\sigma_1-\sigma_3} = \sqrt{3}\tan\theta \qquad \sigma_1 > \sigma_2 > \sigma_3 \tag{8}$$

where θ is Lode's angle. Lode's parameter, μ, was first raised by Walter Lode in 1925 who subjected pipes of various materials (iron, copper, and nickel) to various stress states by means of internal pressure (Lode 1925). Thus, the Lode's parameter, μ, can

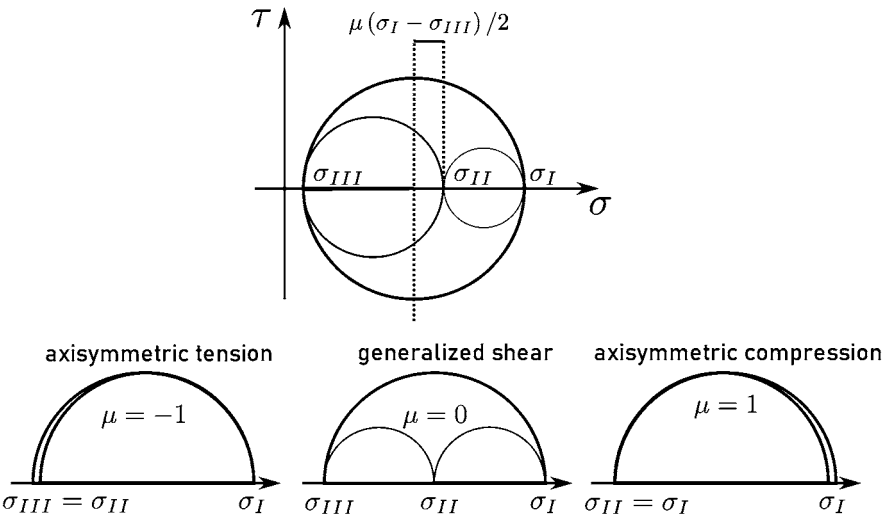

Fig. 2 Representation of the Lode parameter, μ for three cases: tension (μ = − 1); shear (μ = 0); and compression (μ = 1)

be illustrated by Mohr's circle, as shown in Fig. 2, where three cases are founded: tensile (μ = − 1); shear (μ = 0); and compression (μ = 1).

The Lode's angle can be easily related to the third invariant, giving rise to the dimensionless Lode's angle parameter, ξ, as:

$$\xi = \cos\ 3\theta = \frac{27}{2}\frac{J_3}{\overline{\sigma}^3} = \frac{3\sqrt{3}}{2}\frac{J_3}{J_2^{\frac{3}{2}}} \tag{9}$$

The Lode's angle θ can be normalized according to the results of Bai et al. (Bai and Wierzbicki 2008) as:

$$\overline{\theta} = 1 - \frac{6\theta}{\pi} = 1 - \frac{2}{\pi}\ \arccos\ \xi \tag{10}$$

The range of the Lode's parameter, μ, in Eq. 8, and the normalized Lode's angle $\overline{\theta}$, Eq. 10, is $-1 \leq \left(\mu \text{ or } \overline{\theta}\right) \leq 1$. It is important to note that triaxiality is a function of the invariants I_1 and J_2, while Lode's angle is related to the invariants J_2 and J_3.

Damage Models

Generally, the study of the ductile fracture phenomenon has been divided into two types of models: coupled damage models and decoupled damage models.

- *Coupled Damage Model*

The constitutive model and the failure criterion are coupled. They are known as models based on Continuum Damage Mechanics (CDM) which were first developed by Kachanov (1986) and later studied by numerous researchers (Chaboche 1988; Alves and Jones 1999). They describe the degradation of the material with an internal state variable, D (Rice 1971). Thus, failure occurs when the accumulated damage reaches a critical value. A detailed summary of these models can be found at Refs. (Khan and Liu 2012; Brünig 2003; Badreddine et al. 2010).

Some models introduce damage within the plasticity criterion, as in the Gurson model (Gurson 1977) for porous materials. An alternative is to introduce the damage into the hardening law, inducing a progressive weakening (Xue 2007a, b). A realistic physical foundation is presented in these models; however, the calibration of the model parameters is rather complex. For example, the Gurson model requires the identification of nine parameters (Teng 2008).

- *Decoupled Failure Models*

The failure is considered an unforeseen event when the stress and deformational state reach a critical level. The criteria developed by McClintock in 1968 (McClintock 1968) demonstrated that failure strain was related to stress state and void geometry. Rice and Tracey in 1969 (Rice and Tracery 1969) proposed a vacuum growth model to show how the stress state affected void growth (Eq. 11):

$$\overline{\varepsilon}_f^p = \overline{\varepsilon}_f^p(\eta) = C_1 e^{-C_2\,\eta} \tag{11}$$

where C_1 and C_2 are material constants; and η is a parameter that considers the stress state, called *triaxiality*, defined as the ratio between the hydrostatic pressure and the von Mises effective stress.

Initially, numerous studies have shown that failure deformation decreases as triaxiality increases (Hancock and MacKenzie 1975; Johnson and Cook 1985; Le Roy et al. 1981). Following up this research field, Johnson and Cook proposed a failure criterion which is widely used nowadays. To this end, they postulated that equivalent plastic strain to failure $\overline{\varepsilon}_f^p$ is a function of triaxiality η. The damage variable D in the Johnson-Cook criterion is an integral weighting with respect to equivalent plastic strain (Johnson and Cook 1985), as shown in Eq. 12:

$$D = \int_0^{\overline{\varepsilon}_c} \frac{d\overline{\varepsilon}^p}{\overline{\varepsilon}_f\left(\eta, \dot{\overline{\varepsilon}}^p, T\right)} \tag{12}$$

where $\overline{\varepsilon_c}$ is the equivalent critical plastic strain failure value for an applied load. Failure strain in criterion JC is defined by triaxiality, η; plastic strain rate, $\dot{\overline{\varepsilon}}^p$; temperature, T; and five material constants $D_1 - D_5$ as described in Eq. 13:

$$\bar{\varepsilon}_f = \left[D_1 + D_2\, e^{(D_3\,\eta)}\right] \cdot \left[1 + D_4\, \log \frac{\dot{\bar{\varepsilon}}^p}{\dot{\varepsilon}_o}\right] \cdot \left[1 + D_5\, \frac{T - T_0}{T_{melt} - T_0}\right] \tag{13}$$

where T_0 is the ambient or reference temperature and T_{melt} is the melting temperature. In Eq. 13, the effects of pressure (or triaxiality), strain rate, and temperature are expressed as an independent three-component product.

Generally, it is not possible to analyze the effect of the stress state on the effective plastic strain of failure from experimental results in a straightforward manner. This is why numerical-experimental methodologies are needed (Bao 2005; Bao and Wierzbicki 2004a, b, 2003a; Bai et al. 2006; Mohr and Henn 2007). Traditionally, the uniaxial tensile tests are used to obtain failure strains. These tests can be carried out in axisymmetric or in flat specimens, as Brigdman developed in 1952. The research group of Wierzbicki (Bai and Wierzbicki 2008; Wierzbicki et al. 2005; Wierzbicki 2006), Mohr and Henn (Mohr and Henn 2007; Mohr and Ebnoether 2009), Kim et al. (Kim et al. 2003, 2004, 2007), and Gao et al. (Gao et al. 2005, 2009a; Gao and Kim 2006) developed experimental campaigns using different geometries and loading conditions to obtain failure deformation.

In 2004, Bao and Wierzbicki (2004a, b, 2003a) studied the effective plastic deformation at failure in a wide range of triaxialities $\left(-\frac{1}{3} \le \eta < 2\right)$, as shown in Fig. 3, and proposed a criterion that is reflected in Eq. 14:

$$\bar{\varepsilon}_f = \begin{cases} \dfrac{D_1}{1 + 3\eta} + D_2 & \text{if } -1/3 < \eta \le 0 \\ D_3\eta^2 + D_4\eta + D_5 & \text{if } 0 < \eta \le \eta_T \\ D_6 + D_7 e^{-D_6\eta} & \text{if } \eta_T < \eta \end{cases} \tag{14}$$

where η_T is the transition triaxiality.

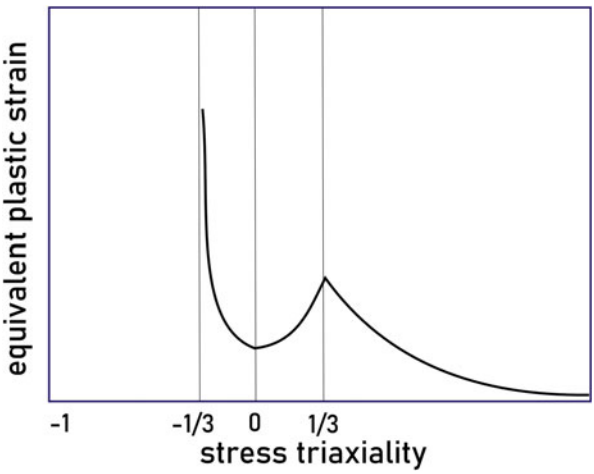

Fig. 3 Dependence of equivalent plastic strain with triaxiality

Bao et al. deduced that, as shown in Fig. 3, the equivalent deformation at failure was not represented by monotonous decreasing function in triaxiality.

Furthermore, these researchers, together with studies by Barsoum and Faleskog in 2007 (Barsoum and Faleskog 2007a), showed that triaxiality was insufficient to adequately describe the behavior of the material under failure conditions. In order to improve the accuracy of the failure prediction criteria and to be able to describe in a more complete way the stress state, the Lode's parameter was introduced. In this regard, Xue et al. (Xue 2007a, b) found that there was a great dependence of the Lode's parameter on ductile failure in metals. Thus, they developed a 3D and symmetrical failure criterion in the space of triaxiality and the third normalized invariant ξ as expressed in Eq. 15. The envelope is shown in Fig. 4b. In addition, the difference between the JC criterion and the Xue-Wierzbicki criterion is shown in Fig. 4, where the dependence of the deformation at failure with the Lode's parameter is clearly observed:

$$\overline{\varepsilon}_f(\eta,\xi) = D_1\, e^{-D_2\,\eta} - \left(D_1\, e^{-D_2\,\eta} - D_3\, e^{-D_4\,\eta}\right)\left(1 - \xi^{1/n}\right) \tag{15}$$

where D_1, D_2, D_3, and D_4 are parameters that must be calibrated and n is the hardening coefficient.

However, the symmetric consideration of the failure criterion may be too restrictive, as it is not based on experimental evidence.

Subsequently, Bai (Bai and Wierzbicki 2008) in 2008 simplified the criterion proposed by Xue, assuming that the behavior of the material followed a Mohr-Coulomb failure criterion. A geometric representation of the 3D failure criterion proposed by Bai and Wierzbicki is shown in Fig. 5.

Therefore, the interest of numerous researchers to study the influence of the stress state (*triaxiality and Lode parameter*) on the equivalent plastic deformation at failure is evident. On the one hand, it has been demonstrated that the equivalent plastic deformation at failure (at high values of triaxiality and considering that the material

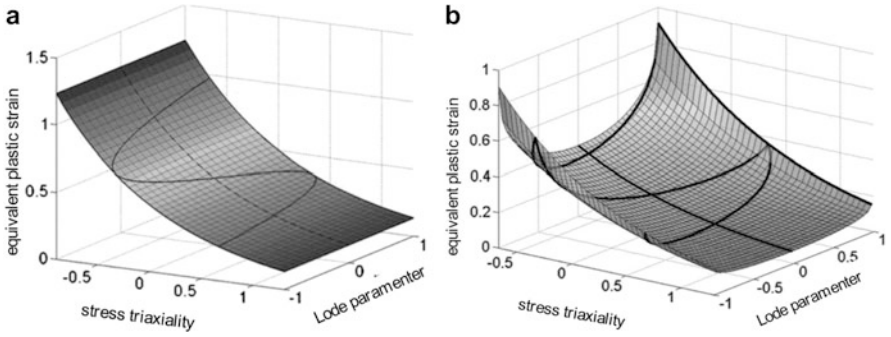

Fig. 4 (**a**) Independent failure criterion of ξ postulated by Johnson and Cook (1985), (**b**) symmetrical 3D failure criterion taking into account ξ postulated by Xue and Wierzbicki (Xue 2007a). (Adapted figure)

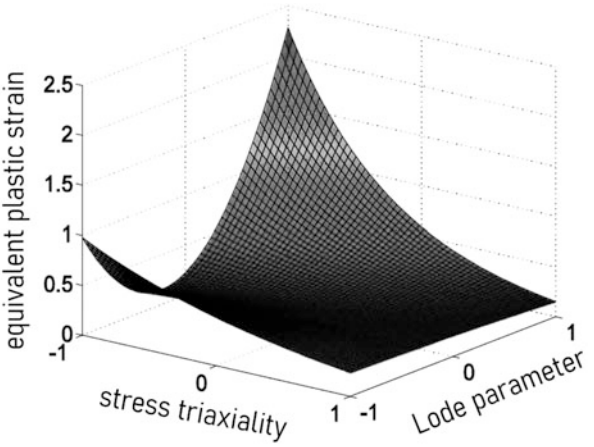

Fig. 5 Failure strain versus triaxiality and Lode parameter proposed by Bai and Wierzbicki (2008) in AA 2024-T351. (Adapted figure)

has a great dependence both on the hydrostatic pressure and the Lode's parameter) decreases when the triaxiality value is increased. This can be explained by the major role played by spherical void growth mechanisms during the damage process (Bao and Wierzbicki 2004a). However, at low triaxiality values, the equivalent plastic strain at failure increases with triaxiality, because void elongation becomes the predominant mechanism (Bao and Wierzbicki 2004a). Nevertheless, Bai et al. (Bai 2008) and Gao et al. (Gao et al. 2009a) found that for materials with a weak dependence on hydrostatic pressure and Lode's parameter, e.g., 1045 steel or 5083-H116 aluminum alloy, the equivalent plastic strain at failure decreased with increasing triaxiality. In particular, for the aluminum alloy AA 5082-H116, Gao et al. (Gao et al. 2009a, 2011a; Graham et al. 2012; Zhao and Holmedal 2012) concluded that triaxiality has a relatively small effect on plasticity but a relevant effect on ductile failure deformation. On the other hand, the effect of Lode's parameter on ductile failure is negligible, while in plasticity its effect is important.

Experimental and Numerical Analysis of Ductile Failure

In general, the calibration of a ductile failure criterion in a wide range of triaxiality and Lode's parameter values requires a large campaign of experimental tests using different specimen geometries and loading conditions (Gao et al. 2009a; Mirone and Corallo 2010; Sun et al. 2009). Seidt (Seidt 2010) used 12.7 mm thick plates to calibrate the ductile failure criteria and performed tensile tests on axisymmetric specimens and plastic plane strain specimens, along with experimental tests of tensile-torsion and pure shear. The triaxiality range obtained by Seidt was from -0.157 to 0.855, and the range of the Lode's parameter was from -0.420 to 1. Studies performed by Gao et al. (2009a, 2011b), using axisymmetric specimens

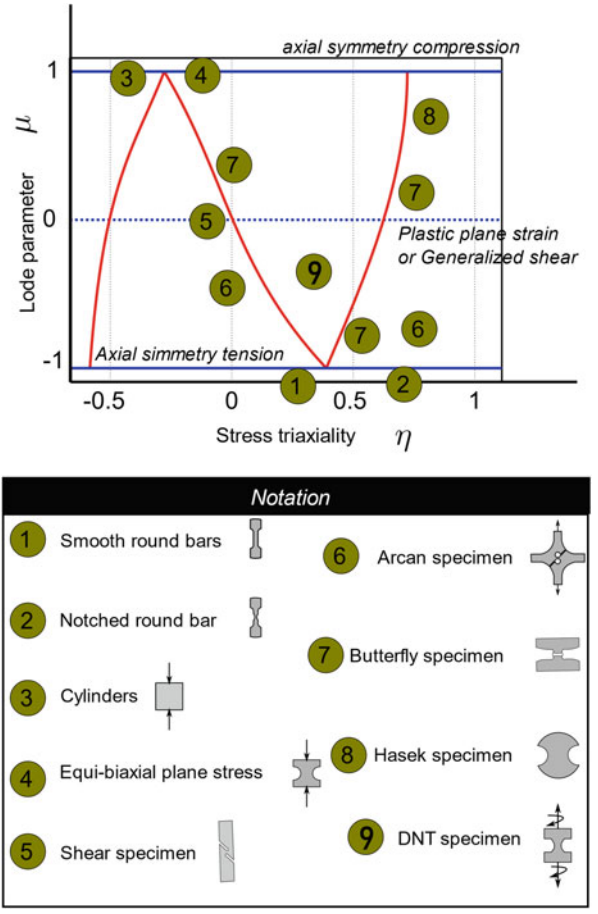

Fig. 6 Conceptual representation of the stress states on the plane of stress triaxiality and Lode parameter

and plastic plane strain specimens, predicted that triaxiality depended not only on the geometry of the specimen but also on the plastic behavior of the material.

The following is a description of the most commonly used specimens in the literature in the calibration of ductile failure criteria. Bai and Wierzbicki (2008) summarized the specimens used in plasticity and fracture that can only be defined by the set of parameters (η, μ). Figure 6 shows the evolution of η and $\overline{\theta}$ where the common essays are shown.

- *Specimens Subjected to Tension Stresses*

  The most commonly used specimens for the calibration of failure criteria under tension stress conditions in literature are presented next:

  – *Cylindrical Axial Symmetry Specimens*

    Tensile tests on bars with different notches are commonly used to investigate the effect of triaxiality on failure deformation (Johnson and Cook 1985; Mackenzie et al. 1977). Bridgman (1935) was the first to analyze the

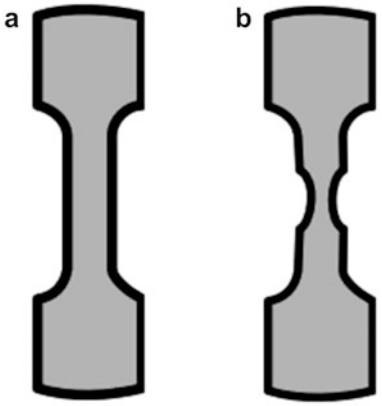

Fig. 7 (**a**) Smooth round bars and (**b**) notched round bar

distribution of stresses in solid bars with different notches and resulted in the expression of triaxiality for the specimen geometry from Fig. 7.

In the center section of the notch, where the fracture begins, Bridgman's expression is:

$$\eta = \frac{1}{3} + \ln\left(1 + \frac{a}{2R}\right) \tag{16}$$

where η is the triaxiality, a is the neck section radius, and R is the neck curvature radius.

The equivalent failure strain for notched axial symmetric bars can be approximated using Eq. 17:

$$\bar{\varepsilon}_f = 2 \ln\left(\frac{a_o}{a_f}\right) \tag{17}$$

The Bridgman's formula and the failure formula are frequently used to calibrate the parameters of the failure criterion (Rice and Tracery 1969; Johnson and Cook 1985; Børvik et al. 2002). However, the lack of consideration of Lode's parameter introduces several difficulties when using this calibration on smooth or notched bars. In this regard, the range of stress state parameters in smooth or notched specimens is $\eta \geq ⅓$ and $\bar{\theta} = 1$ ($\mu = -1$).

– *Grooved Flat Specimens*

Grooved flat specimen is a geometry developed to obtain plastic plane strain states, which corresponds to a Lode's parameter of $\mu = 0$, where the main strain component in the width direction is very small compared to the other two main deformation components. By changing the radius of the notch, different triaxiality values can be obtained for a constant Lode's parameter $\mu = 0$.

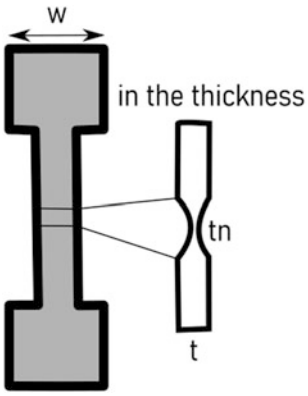

Fig. 8 Grooved flat specimen

To ensure plane strain conditions, the specimens must be properly dimensioned, since the thickness t, width w, and the minimum thickness of the center of the notch t_m (Fig. 8) have a remarkable influence on the stress state. Bai and Wierzbicki used ratios of $w/t_m = 33.25$ and $t/t_m = 3.125$; Benzerga used ratios of $w/t_m = 16.6$ and $t/t_m = 3.0$; and Basaran (2011) performed a numerical study in which they observed that the ratio w/t_m has a significant influence on the evolution of Lode's parameter with plastic strain and that for values greater than $w/t_m = 12.5$, plane strain conditions are obtained. Thus, ratios of $w/t_m = 12.5$ and t/t_m = 2.5 were used.

The analytical expression, Eq. 18, shows that for plane strain plates with or without slots, the loading conditions are $\eta \geq \frac{1}{\sqrt{3}}$ and $\overline{\theta} = 0$ due to the plane strain condition. Comparing notched and smooth bars, the triaxiality range is the same as in slotted plates but with a different $\overline{\theta}$ value. So, Bai and Wierzbicki postulated the expression in Eq. 18 for slotted plates in flat deformation:

$$\eta = \frac{\sqrt{3}}{3}\left[1 + 2\ \ln\left(1 + \frac{a}{2R}\right)\right] = \frac{\sqrt{3}}{3}\left[1 + 2\ \ln\left(1 + \frac{t}{4R}\right)\right] \tag{18}$$

where t is the thickness on the plate. This equation implies that triaxiality is $\eta \geq 1/\sqrt{3}$. In addition, it can be shown that Lode's parameter is zero. The equivalent failure strain in the neck section for a slotted plate like the one in Fig. 19 is defined as:

$$\overline{\varepsilon_f} = \frac{2}{\sqrt{3}} \ln\left(\frac{t_0}{t_f}\right) \tag{19}$$

where t_0 is the initial thickness of the slot and t_f is the fracture thickness.

– *Dog-Bone Specimen*

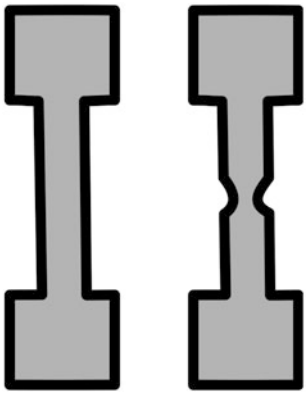

Fig. 9 Dog-bone specimen

The tests with dog-bone specimen (Fig. 9) provide failure strains for high triaxiality values. Triaxiality is a function of the radius of the notch (Eq. 20). For large notch radii, the stress state in the center of the test tube (where strictness occurs) corresponds to uniaxial tension, while the plane strain condition (along the direction of width) is achieved for very small notch radii. In the case of isotropic materials, the variation of the stress state corresponds to a range of triaxial values from 0.33 to 0.58:

$$\eta = \frac{1 + 2\Lambda}{3\sqrt{\Lambda^2 + \Lambda + 1}} \tag{20}$$

where $\Lambda = \left(1 + \frac{t}{4R}\right)$, with R being the radius of the notch and t the thickness of the plate.

- *Specimens Subjected to Compression Stress*

  The most commonly used specimens for the calibration of failure criteria under compression stress conditions in literature are the conventional cylindrical specimen, the notched cylindrical specimen, and the flat specimen whose characteristics are listed below:

  – *Cylinders Compression Test*

    One of the most frequent tests to study fracture is the uniaxial compression test of small cylinders (Fig. 10) using two perfectly horizontal plates. Due to friction between the specimen and the two plates, the barrelling effect occurs during the test about half of the specimen. The test of these specimens provides failure strains for a negative triaxiality range. Depending on the ratio between diameter and cylinder height, different triaxial values are obtained. Bao and Wierzbicki (2003a) used different specimen dimensions and obtained triaxiality values from -0.278 to -0.2235 and Lode parameter from 0.625 to 0.821.

    Friction plays an important role in the *barrelling effect* and in the fracture, which entails a certain difficulty in the realization of numerical simulations.

Fig. 10 Cylinders

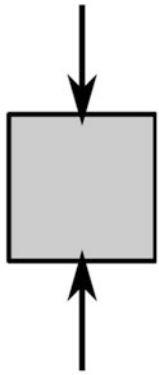

– *Notched Cylinders*

The specimen has a cylindrical geometry with a circular notch in the middle of the height, which causes the deformation to be very localized (Fig. 11). It also avoids the undesirable friction effect that originated in conventional compression specimens.

– *Plane Stress*

Recently, Beese and Mohr (Experimental Investigation 2011) developed a device capable of performing compression tests on flat specimens (Fig. 12). The main problem when performing compression tests on flat specimens is the buckling of the specimen axis. Based on previous studies, these authors developed a device capable of avoiding this phenomenon. They also modified the initial geometry of the specimen and proposed a procedure to correct the effects of friction. This procedure was validated with conventional compression specimens (*for more details see (*Experimental Investigation 2011*)*). This specimen geometry has been used for plasticization, although it is foreseeable that it has a great utility to obtain values of triaxiality – *in a negative regime* – and Lode parameter.

- *Specimens Subjected to Shear*

The main specimens subjected to shear are the notched one at 45º and the Arcan specimen whose characteristics are listed below:

– *Shear Specimens*

Shear specimens tested under tension allow to obtain pure shear states in the central zone associated with triaxiality values close to zero. The geometry is shown in Fig. 13.

To obtain information on the dependence of triaxiality on the behavior of the material for low triaxiality values, shear specimens are developed with a notch out of the plane between the two central holes.

– *Arcan Specimens*

The specimen was modified by Driemeier et al. (2010) is used to obtain information on the material behavior depending on triaxiality. Details of the

Fig. 11 Notched cylinder

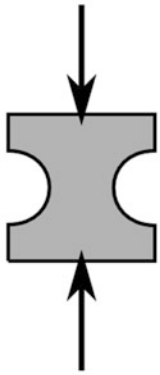

Fig. 12 Plane stress specimens

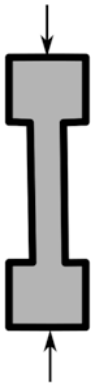

geometry are shown in Fig. 14. This geometry allows for deformations at low, $\eta \approx 0$, *similar to shear specimens*, and high, $\eta > 0.4$, *similar to notched specimens*, triaxiality values depending on the loading direction (Fig. 14). The specimen thickness must be large enough to prevent instabilities due to torsional buckling during the test – Driemeier et al. considered using a specimen thickness of 6.35 mm.

Experimental tests with this specimen geometry can be used to analyze the effect of hydrostatic pressure on the material behavior. However, the effect of the Lode's parameter in the case of plane stress cannot be studied because it depends on triaxiality and is not an independent variable.

- *Equibiaxial Test: Butterfly Specimen*

  Wierzbicki et al. (2005) developed a specimen in the form of a *butterfly* (Fig. 15), which is tested by combining tension and shear to investigate failure at low triaxiality values. This specimen is designed in such a way that the highest strains are located in its central zone, locally increasing the probability of fracture. The length for the calculation section in the central zone is the smallest, as it

Fig. 13 Shear specimen

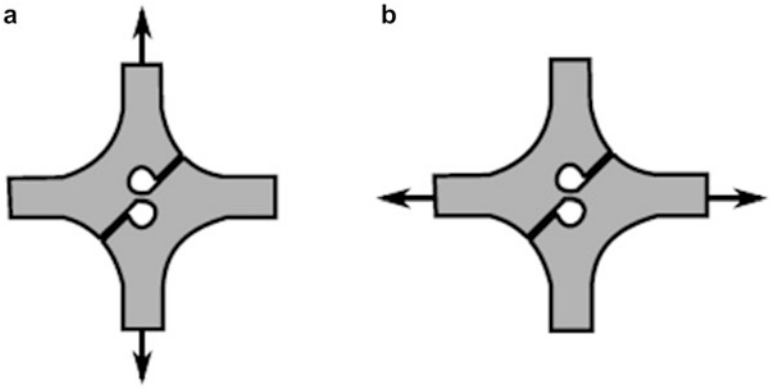

Fig. 14 Arcan specimen. (**a**) Low triaxiality, shear; (**b**) high triaxiality, tension

increases towards the free edges of the specimen. The range of triaxial values and Lode's parameter that can be achieved is $-0.191 \leq 1.01$ and $-0.858 \leq 0.503$; however, it requires a complex experimental device and the manufacture of a complicated specimen to perform the tests. The clamping of the test piece is shown in Fig. 15. The tests performed with this specimen are suitable only for validation, not for calibrating failure criteria (Beese et al. 2010).

- *Punch Tests*

  Punch test or Hasek tests (1978) are normally used to evaluate deformation under biaxial conditions in metal sheets. In this test, a circular flat specimen is embedded in its contour and subjected to the impact of a rigid penetrator by means of a drop tower device (Fig. 16). A lubricant is usually used between the impactor and the sheet metal to avoid possible friction effects. By changing the geometry of the sheet metal, a range of tension state can be covered between uniaxial tension $\left(\eta = \frac{1}{3}, \mu = -1\right)$ and equibiaxial tension ($\eta = 2/3, \quad \mu = \ -\ 1$) (Walters 2009).

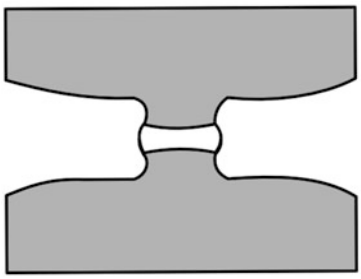

Fig. 15 Butterfly specimen

The modification of the specimen's geometry in this type of test allows to obtain different stress states (Fig. 17). Thus, an increase in the circular notch radius, R_n, means a decrease in triaxiality and an increase in the Lode parameter.

- *Test with Modified Shear Specimen*

  By changing the shape of the notch section of the pure shear specimen in such a way that it induces a stress state of combined tension-shear, Fig. 18. With this geometry a triaxiality interval from 0 to 0.4 is achieved (Bao and Wierzbicki 2004a).

- *Combined Tensile-Torsion Tests*

  This type of test consists of subjecting the specimen to combined tension-torsion states in a simultaneous manner. It is worth mentioning the double-notch tubular specimen and the Lindholm tubular specimen, whose characteristics are defined below:

  – *Double-Notch Tubular Specimen*

    Barsoum and Faleskog (Barsoum and Faleskog 2007b; Barsoum et al. 2012) developed the double-notched tube specimen (Fig. 19) to carry out tests in a range from low to medium triaxiality. This type of specimens is loaded with combined tension and torsion maintaining a constant that regulates triaxiality. With this specimen geometry, you can obtain variations in triaxiality in a range of $(0 \leq \eta \leq 1.1)$ and of the Lode parameter in an interval of $(-1 \leq \mu \leq 0)$ using the same specimen geometry. Both the evolution of triaxiality and the Lode parameter are calculated at the center of the notch during the loading process using numerical simulations.

    Recently, three different aluminum alloys (5754-H111, 6082-T6, and 2024-T3) have been studied to analyze the influence of the stress triaxiality and Lode parameter on the failure strain (Rodríguez-Millán et al. 2015, 2018a) (Fig. 20). Rodríguez-Millán et al. (2015, 2018a) concluded that the failure strain was not monotonic with decreasing triaxiality in all cases. In fact, in the case of AA 2024, a maximum peak is reached for a triaxiality threshold of $\mu \sim 0.68$ and then decreases again. A similar behavior is found in AA 5754-H111, with a

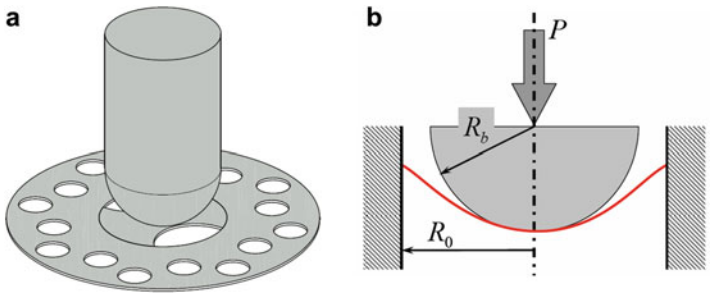

Fig. 16 Punch test

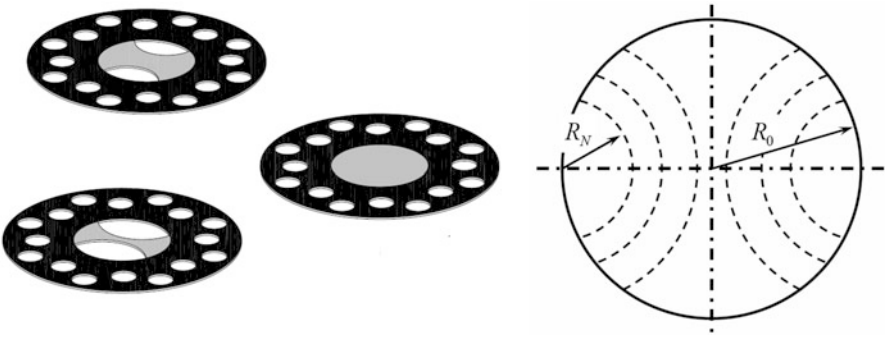

Fig. 17 Types of specimens for dynamic punch tests. Modification of the radius R_n of circular notch allows to obtain different values of the triaxiality and the Lode parameter

Fig. 18 Modified shear specimen

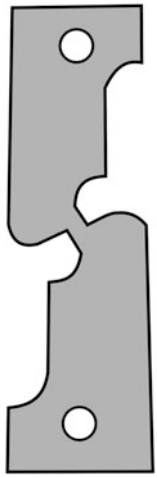

peak value of 0.8. According to several researchers, this behavior can be explained by means of the Lode parameter (Bao and Wierzbicki 2003b).

Void growth and coalescence are the dominant failure mechanisms at high triaxialities, while at low triaxialities shearing between voids becomes the main failure mechanism. These behaviors do not occur in all materials. In this regard, there are examples in the literature where certain metals have a low dependence on the third invariant (Lode parameter), such as 5083-H116 aluminum alloy (Gao et al. 2009b) or DH36 steel (Gao et al. 2010).

Among the three aluminum alloys studied by Rodriguez-Millan and collaborators, AA 5754-H111 showed the highest failure strain, while 6082-T6 presented the lowest values. The maximum values of failure strain for AA 2024-T3 and 5754-H111 were identified to be tensile failure mechanisms, while for AA 6082-T6, the maximum values were determined to be shearing mechanisms. The low influence of the Lode parameter on AA 6082-T6 is similar to that shown by Zhou and collaborators (2012).

The experimental tests conducted by Rodriguez-Millan and co-authors (2014, 2018b) revealed relevant insights into the mechanical performance of three different aluminums (in terms of strength and hardening): AA 2024 shows the highest values for both terms, while AA5754 has a low strength and moderate hardening; AA 6082 presents intermediate values of strength and hardening. As Barsoum et al. (2012) demonstrated, the influence of the Lode parameter increases with the yield stress accompanied by a decrease in hardening.

– *Modified Lindholm Specimen*

Gao et al. (2011b) developed an alternative design to the double-notch tubular specimen used by Faleskog et al. The specimen is a modification to the specimen used by Lindholm et al. (Lindholm 1980) for experimental torsion tests at high strain rate. The dimensions of the specimen are shown in Fig. 21. The main differences with the geometry developed by Lindholm are that the length is longer and the ends are cylindrical rather than hexagonal.

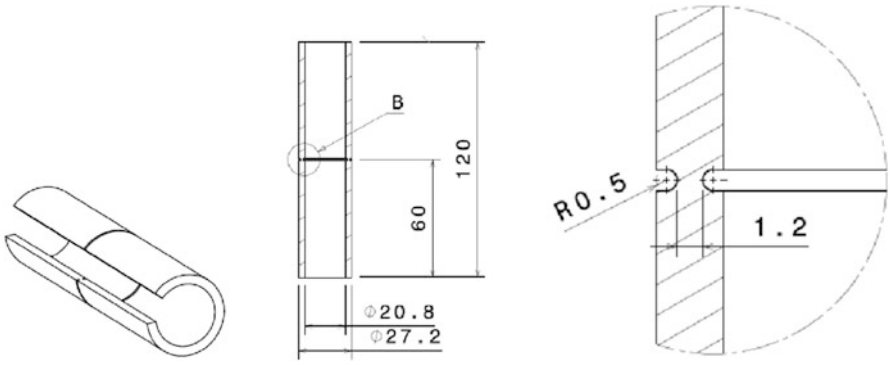

Fig. 19 Double-notch tubular specimen

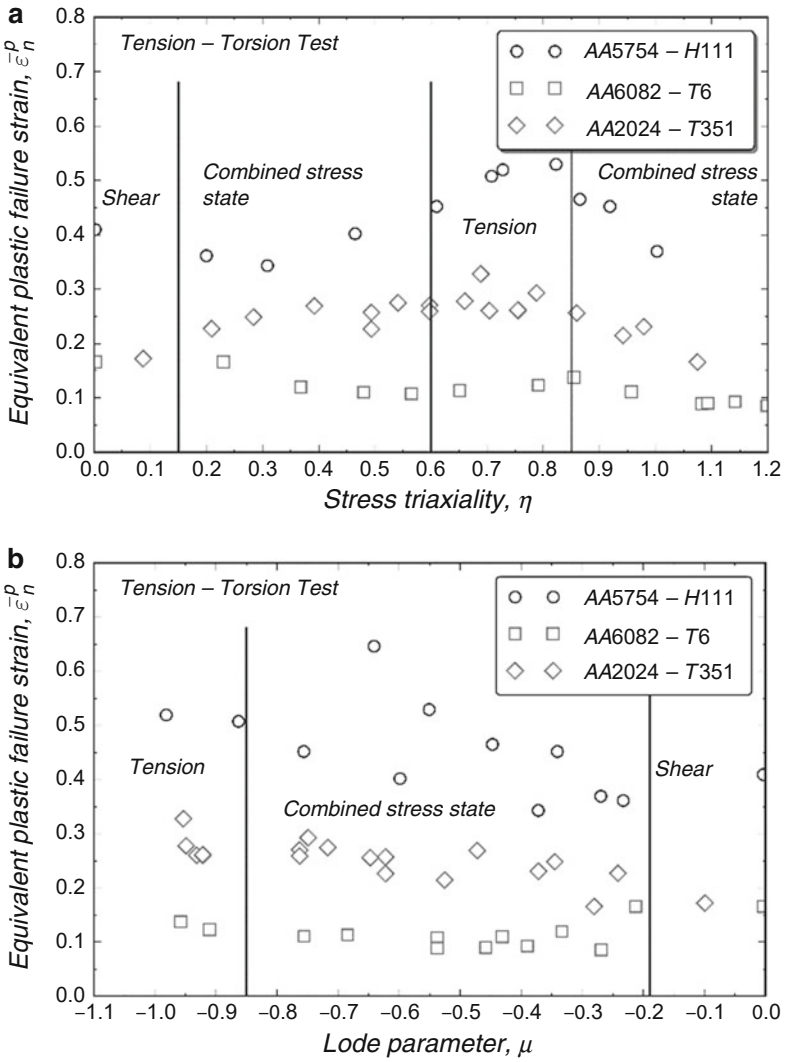

Fig. 20 Failure locus on the space of equivalent plastic strain versus: (**a**) stress triaxiality; (**b**) Lode parameter

The modified Lindholm specimen is quite similar to the double-notch tubular specimen; they are the same size, but the sections are significantly different. The specimen developed by Barsoum has both internal and external circular notches, while the modified Lindholm specimen has a single notch on the outside with a trapezoidal groove profile. The height of the notch in the modified Lindholm specimen is 2.54 mm, while in the double-notch specimen, it is circular radius 0.5 mm. The notch width in the double-notch specimen is

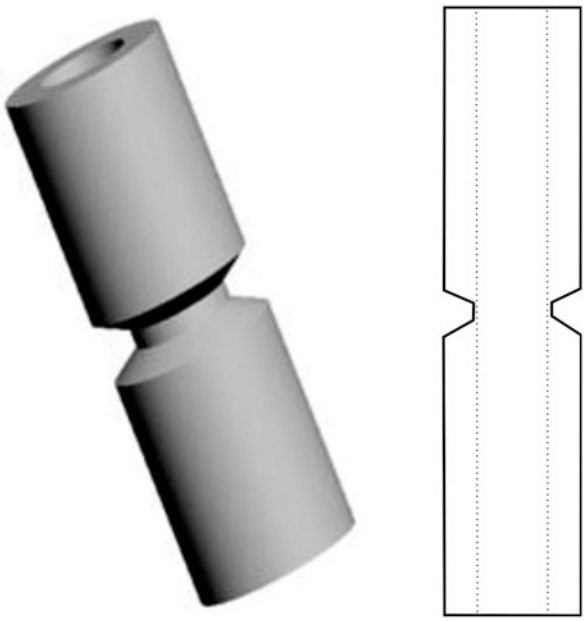

Fig. 21 Modified Lindholm specimen and its transversal area

1.2 mm at the narrowest point, which is approximately twice the thickness of the notch in the Lindholm specimen (~0.74 mm).

As the geometry of both specimens is different, the same values of triaxiality and Lode's parameter cannot be achieved with the same state of tensile and torsional loads. As shown in Fig. 22, different ranges of triaxiality and Lode's parameter values are obtained depending on the geometry of the specimen for the same material. Thus, the behavior of the Lindholm specimen covers an interval of $\eta = 0$ and $\mu = 0$, in pure torsion, passing through a state close to that obtained in tension in flat specimens ($\eta = 0.33$ and $\mu = -1$), until obtaining a biaxial state of tension ($\sigma_1 = 2\sigma_2$ and $\sigma_3 = 0$) where $\eta = 0.58$ and $\mu = 0$.

Summary/Conclusions

An analysis of the most common specimens used for characterization of the influence of the stress state on the ductile fracture of metals has been described in this chapter. To this end, the relation between different specimens' geometry and stress states has been presented to obtain tensile, compressive, shear, and mixed states. The wide variety of geometries and their influence on the determination of failure deformation has been proven. These dependences are of critical relevance to determine the fracture process of different components and need to be accounted for modelling tools tackling this problem. In this regard, the stress state dependence on

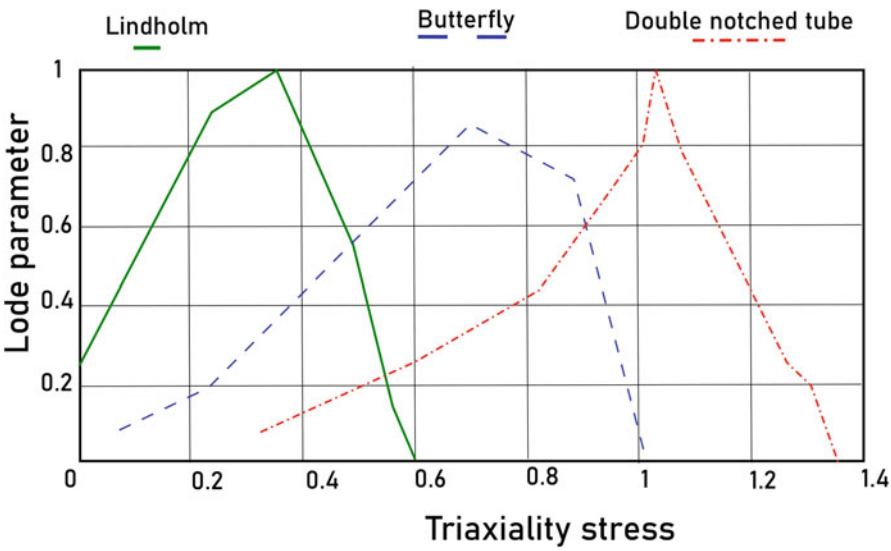

Fig. 22 Comparison of the values of triaxiality and Lode parameter for the modified Lindholm specimens, the butterfly specimen, and double-notch tubular specimen

failure deformation is still an open problem where further efforts must be done to incorporate temperature and deformation rate dependences.

References

M. Alves, N. Jones, Influence of hydrostatic stress on failure of axisymmetric notched specimens. J. Mech. Phys. Solids **47**, 643–667 (1999)

H. Badreddine, K. Saanouni, A. Dogui, On non-associative anisotropic finite plasticity fully coupled with isotropic ductile damage for metal forming. Int. J. Plast. **26**, 1541–1575 (2010). https://doi.org/10.1016/j.ijplas.2010.01.008

Y. Bai, *Effect of Loading History on Necking and Fracture* (Massachusetts Institute of Technology, 2008)

Y. Bai, T. Wierzbicki, a new model of metal plasticity and fracture with pressure and Lode dependence. Int. J. Plast. **24**, 1071–1096 (2008). https://doi.org/10.1016/j.ijplas.2007.09.004

Y. Bai, Y. Bao, T. Wierzbicki, Fracture of prismatic aluminum tubes under reverse straining. Int. J. Impact Eng. **32**, 671–701 (2006). https://doi.org/10.1016/j.ijimpeng.2005.05.002

Y. Bao, *Prediction of Ductile Crack Formation in Uncracked Bodies* (2003)

Y. Bao, Dependence of ductile crack formation in tensile tests on stress triaxiality, stress and strain ratios. Eng. Fract. Mech. **72**, 505–522 (2005). https://doi.org/10.1016/j.engfracmech.2004.04.012

Y. Bao, T. Wierzbicki, *Prediction of Ductile Crack Formation in Uncracked Bodies* (Massachusetts Institute of Technology, 2003a)

Y. Bao, T. Wierzbicki, *Prediction of Ductile Crack Formation in Uncracked Bodies* (Massachusetts Institute of Technology, 2003b).

Y. Bao, T.A. Wierzbicki, Comparative study on various ductile crack formation criteria. J. Eng. Mater. Technol. **126**, 314 (2004a). https://doi.org/10.1115/1.1755244

Y. Bao, T. Wierzbicki, On fracture locus in the equivalent strain and stress triaxiality space. Int. J. Mech. Sci. **46**, 81–98 (2004b). https://doi.org/10.1016/j.ijmecsci.2004.02.006

I. Barsoum, J. Faleskog, Rupture mechanisms in combined tension and shear – experiments. Int. J. Solids Struct. **44**, 1768–1786 (2007a). https://doi.org/10.1016/j.ijsolstr.2006.09.031

I. Barsoum, J. Faleskog, Rupture mechanisms in combined tension and shear – experiments. Int. J. Solids Struct. **44**, 1768–1786 (2007b). https://doi.org/10.1016/j.ijsolstr.2006.09.031

I. Barsoum, J. Faleskog, S. Pingle, The effect of stress state on ductility in the moderate stress triaxiality regime of medium and high strength steels. Int. J. Mech. Sci., 1–10 (2012). https://doi.org/10.1016/j.ijmecsci.2012.10.003

M. Basaran, *Stress State Dependent Damage Modeling with a Focus on the Lode Angel Influence* (2011)

A.M. Beese, M. Luo, Y. Li, Y. Bai, T. Wierzbicki, Partially coupled anisotropic fracture model for aluminum sheets. Eng. Fract. Mech. **77**, 1128–1152 (2010). https://doi.org/10.1016/j.engfracmech.2010.02.024

T. Børvik, M. Langseth, O.S.S. Hopperstad, K.A. Malo, T. Berstad, Perforation of 12 mm thick steel plates by 20 mm diameter projectiles with flat, hemispherical and conical noses part II: numerical simulations. Int J Impact Eng **27**, 37–64 (2002)

P.W. Brigdman, Theoretically interesting aspects of high pressure phenomena. Rev. Mod. Phys. **7**, 1–33 (1935)

M. Brünig, An anisotropic ductile damage model based on irreversible thermodynamics. Int. J. Plast. **19**, 1679–1713 (2003). https://doi.org/10.1016/S0749-6419(02)00114-6

J. Chaboche, Continuum damage mechanics: part I-general concepts. J. Appl. Mech. **55**, 59–64 (1988)

L. Driemeier, M. Brünig, G. Micheli, M. Alves, Experiments on stress-triaxiality dependence of material behavior of aluminum alloys. Mech. Mater. **42**, 207–217 (2010). https://doi.org/10.1016/j.mechmat.2009.11.012

A.M. Beese, Experimental investigation and constitutive modeling of the large deformation behavior of anisotropic steel sheets undergoing strain-induced phase. Transformation (2011)

X. Gao, J. Kim, Modeling of ductile fracture: significance of void coalescence. Int. J. Solids Struct. **43**, 6277–6293 (2006). https://doi.org/10.1016/j.ijsolstr.2005.08.008

X. Gao, T. Wang, J. Kim, On ductile fracture initiation toughness: effects of void volume fraction, void shape and void distribution. Int J Solids Struct **42**, 5097–5117 (2005). https://doi.org/10.1016/j.ijsolstr.2005.02.028

X. Gao, T. Zhang, M. Hayden, C. Roe, Effects of the stress state on plasticity and ductile failure of an aluminum 5083 alloy. Int. J. Plast. **25**, 2366–2382 (2009a). https://doi.org/10.1016/j.ijpla1s.2009.03.006

X. Gao, T. Zhang, M. Hayden, C. Roe, Effects of the stress state on plasticity and ductile failure of an aluminum 5083 alloy. Int. J. Plast. **25**, 2366–2382 (2009b). https://doi.org/10.1016/j.ijplas.2009.03.006

X. Gao, G. Zhang, C. Roe, A study on the effect of the stress state on ductile fracture. Int J Damage Mech **19**, 75–94 (2010). https://doi.org/10.1177/1056789509101917

X. Gao, T. Zhang, J. Zhou, S.M. Graham, M. Hayden, C. Roe, On stress-state dependent plasticity modeling: significance of the hydrostatic stress, the third invariant of stress deviator and the non-associated flow rule. Int. J. Plast. **27**, 217–231 (2011a). https://doi.org/10.1016/j.ijplas.2010.05.004

X. Gao, T. Zhang, J. Zhou, S.M. Graham, M. Hayden, C. Roe, On stress-state dependent plasticity modeling: significance of the hydrostatic stress, the third invariant of stress deviator and the non-associated flow rule. Int. J. Plast. **27**, 217–231 (2011b). https://doi.org/10.1016/j.ijplas.2010.05.004

W.M. Garrison Jr., N.R. Moody, Ductile Fracture. J. Phys. Chem. Solids **48**, 1035–1074 (1987)

S.M. Graham, T. Zhang, X. Gao, M. Hayden, Development of a combined tension–torsion experiment for calibration of ductile fracture models under conditions of low triaxiality. Int. J. Mech. Sci. **54**, 172–181 (2012). https://doi.org/10.1016/j.ijmecsci.2011.10.007

A.L. Gurson, Continuum theory of ductile rupture by void nucleation and growth: part I – yield criteria and flow rules for porous ductile media. J. Eng. Mater. Technol. **99**, 2–15 (1977). https://doi.org/10.1115/1.3443401

J. Hancock, A. MacKenzie, On the mechanism of ductile failure in high-strength steels subjected to multi-axial stress-states. J. Mech. Phys. Solids **24**, 147–169 (1975)

G.R. Johnson, W.H. Cook, Fracture characteristics of three metals subjected to various strains, strain rates, temperatures and pressures. Eng. Fract. Mech. **21**, 31–48 (1985)

L. Kachanov, On creep stresses in a Bridgman notched bar. Mech. Mater. **5**, 229–234 (1986). https://doi.org/10.1016/0167-6636(86)90020-7

A.S. Khan, H. Liu, Strain rate and temperature dependent fracture criteria for isotropic and anisotropic metals. Int. J. Plast. **37**, 1–15 (2012). https://doi.org/10.1016/j.ijplas.2012.01.012

J. Kim, X. Gao, T.S. Srivatsan, Modeling of crack growth in ductile solids: a three-dimensional analysis. Int. J. Solids Struct. **40**, 7357–7374 (2003). https://doi.org/10.1016/j.ijsolstr.2003.08.022

J. Kim, X. Gao, T.S. Srivatsan, Modeling of void growth in ductile solids: effects of stress triaxiality and initial porosity. Eng. Fract. Mech. **71**, 379–400 (2004). https://doi.org/10.1016/S0013-7944(03)00114-0

J. Kim, G. Zhang, X. Gao, Modeling of ductile fracture: application of the mechanism-based concepts. Int. J. Solids Struct. **44**, 1844–1862 (2007). https://doi.org/10.1016/j.ijsolstr.2006.08.028

G. Le Roy, J.D. Embury, G. Edward, Ashby MF. A model of ductile fracture based on the nucleation and growth of voids. Acta Metall. **29**, 1509–1522 (1981)

A. Lindholm, Large strain high strain rate testing of copper. J. Eng. Mater. Technol. **102**, 376–381 (1980)

V.W. Lode, Versuche uber den einflub der mittleren hauptspannug auf die fliebgrenze. Zeitschrift Fur Angew Math Und Mech **5**, 142–144 (1925)

A.C. Mackenzie, J.W. Hancock, D.K. Brown, On the influence of state of stress on ductile failure initiation in high strength steels. Eng. Fract. Mech. **9**, 167–188 (1977). https://doi.org/10.1016/0013-7944(77)90062-5

F.A.A. McClintock, Criterion for ductile fracture by the growth of holes. J. Appl. Mech. **32**, 363–372 (1968)

F.A. McClintock, S.M. Kaplan, C.A. Berg, Ductile fracture by hole growth in shear bands. Int. J. Fract. Mech. **2**, 614–644 (1966)

G. Mirone, D. Corallo, A local viewpoint for evaluating the influence of stress triaxiality and Lode angle on ductile failure and hardening. Int. J. Plast. **26**, 348–371 (2010). https://doi.org/10.1016/j.ijplas.2009.07.006

D. Mohr, F. Ebnoether, Plasticity and fracture of martensitic boron steel under plane stress conditions. Int. J. Solids Struct. **46**, 3535–3547 (2009). https://doi.org/10.1016/j.ijsolstr.2009.05.011

D. Mohr, S. Henn, Calibration of stress-triaxiality dependent crack formation criteria: a new hybrid Experimental–numerical method. Exp. Mech. **47**, 805–820 (2007). https://doi.org/10.1007/s11340-007-9039-7

J.R. Rice, Inelastic constitutive relations for solids: an internal-variable theory and its application to metal plasticity. J. Mech. Phys. Solids **19**, 433–455 (1971). https://doi.org/10.1016/0022-5096(71)90010-X

J.R. Rice, D.M. Tracery, On the ductile enlargement of voids in triaxial stress fields. J. Mech. Phys. Solids **17**, 201–217 (1969)

M. Rodríguez-Millán, A. Vaz-Romero, A. Rusinek, J.A. Rodríguez-Martínez, A. Arias, Experimental study on the perforation process of 5754-H111 and 6082-T6 Aluminium plates subjected to Normal impact by conical, hemispherical and blunt projectiles. Exp. Mech. **54**, 729–742 (2014). https://doi.org/10.1007/s11340-013-9829-z

M. Rodríguez-Millán, Á. Vaz-Romero, Á. Arias, Failure behavior of 2024-T3 aluminum under tension-torsion conditions. J. Mech. Sci. Technol. **29**, 4657–4663 (2015). https://doi.org/10.1007/s12206-015-1011-3

M. Rodriguez-Millan, D. Garcia-Gonzalez, A. Rusinek, A. Arias, Influence of stress state on the mechanical impact and deformation behaviors of aluminum alloys. Metals (Basel) **8**, 520 (2018a). https://doi.org/10.3390/met8070520

M. Rodriguez-Millan, D. Garcia-Gonzalez, A. Rusinek, F. Abed, A. Arias, Perforation mechanics of 2024 aluminium protective plates subjected to impact by different nose shapes of projectiles. Thin-Walled Struct. **123**, 1–10 (2018b). https://doi.org/10.1016/j.tws.2017.11.004

J.D. Seidt, *Plastic Deformation and Ductile Fracture of 2024-T351 Aluminum under Various Loading Conditions* (The Ohio State University, 2010)

X. Sun, K.S. Choi, A. Soulami, W.N. Liu, M.A. Khaleel, On key factors influencing ductile fractures of dual phase (DP) steels. Mater. Sci. Eng. A **526**, 140–149 (2009). https://doi.org/10.1016/j.msea.2009.08.010

X. Teng, Numerical prediction of slant fracture with continuum damage mechanics. Eng. Fract. Mech. **75**, 2020–2041 (2008). https://doi.org/10.1016/j.engfracmech.2007.11.001

C.L. Walters, *Development of a Punching Technique for Ductile Fracture Testing Over a Wide Range of Stress States and Strain Rates* (Massachusetts Institute of Technology, 2009)

T. Wierzbicki, *Fracture of Advance High Strength Steels (AHSS)* (2006:48)

T. Wierzbicki, Y. Bao, Y.-W. Lee, Y. Bai, Calibration and evaluation of seven fracture models. Int. J. Mech. Sci. **47**, 719–743 (2005). https://doi.org/10.1016/j.ijmecsci.2005.03.003

L. Xue, Damage accumulation and fracture initiation in uncracked ductile solids subject to triaxial loading. Int. J. Solids Struct. **44**, 5163–5181 (2007a). https://doi.org/10.1016/j.ijsolstr.2006.12.026

L. Xue, *Ductile fracture modeling - theory, Experimental Investigation and numerical verification* (Massachusetts Institute of Technology, 2007b)

Q. Zhao, B. Holmedal, The effect of silicon on the strengthening and work hardening of aluminum at room temperature. Mater. Sci. Eng. A (2012). https://doi.org/10.1016/j.msea.2012.11.062

J. Zhou, M. Hayden, X. Gao, An investigation of the strain rate and temperature effects on the plastic flow stress and ductile failure strain of aluminum alloys 5083-H116, 6082-T6 and a 5183 weld metal. Proc Inst Mech Eng part C. J. Mech. Eng. Sci. (2012). https://doi.org/10.1177/0954406212450962